35th Annual International Conference of the IEEE EMBS
Osaka, Japan, 3 - 7 July, 2013

Pleura Detection in Chest Computed Tomography with Application for Nodule Detection

Shuo-Chueh Chen, Su-Tso Yang, Yang-Hao Yu, Chih-Yi Chen, and Wei-Chih Shen

Abstract— **This paper proposes an efficient algorithm for detecting pleural objects that come in contact with a nodule. To reduce complexity, the algorithm recursively performed a curve-fitting method on each slice of the volume of interest to locate the object between the parietal and visceral pleurae surfaces and measured the quality of the fitting curve. When a nodule contacted the surfaces of the chest wall or diaphragm, they were automatically separated using the fitting curve. The algorithm was performed on 864 slices of 40 nodules. The segmentation results were visually inspected by a consensus of attending physicians to search for any segmentation errors. The consensus accepted 93.6% of the segmentation results.**

I. Introduction

Mortality from lung cancer is reduced by screening individuals using low-dose computed tomography (CT) [1]. The density characteristic of nodule is commonly represented as either ground-glass opacity (GGO) or partially GGO in the screening [2]. The GGO is defined as a hazy increased attenuation of the lung tissue and does not obscure underlying bronchioles and blood vessels [3]. The size measurements of the GGO nodules are diverse among physicians [4] because of the outline is ambiguous. Computer-aided detection (CADe) methods for detecting pulmonary nodules in CT images then becomes a novel challenge.

The relationship between the nodule and the pleural objects surrounding the lung tissue mainly affects the performance of the CADe methods. Pleural invasion, indicating that a nodule contacted and invaded the surface of a chest wall or diaphragm, occurs in approximately 8% of patients with a pulmonary malignancy [5]. When a nodule is adjacent to or contacts the surface of pleural objects, separation is necessary for analysis. In template-based methods [6][7], a semicircle for detecting the nodule attached to the chest wall is defined to search for structures with similar properties. Based on the contrast between the sensitivity of the local adaptive segmentation and small local differences, the nodules can be separated from the chest wall, despite their intensities being similar [8]. Based on the combination of intensity and geometric models, Paik et al. proposed a surface normal overlap method to identify the lesion on the chest wall [9].

This study proposes a pleura detection algorithm for finding the location of the pleura between the lung tissue and its surrounding structures. When considering the applications of nodule detection, especially for GGO nodules, pleura detection can be used as a preprocess. The obvious difference between pleural objects and lung tissue mainly decided a threshold for classifying foreground and background objects in CT images; but, the threshold is generally overestimated for GGO nodules. The exclusion of pleural objects improved the performance to measure the threshold for detecting the GGO nodules. The contact area between the nodule and pleural objects provided efficient information to evaluate the pleural invasion.

II. Materials and Basic Definitions

All CT images were shown using the lung window setting with center -600 HU and width 1600 HU; that is, the CT attenuations between -1400 and 200 HU were transformed into gray scale between 0 and 255 for display. The proposed algorithm was performed using the original CT attenuation rather than the gray scale.

Two measurements were employed to evaluate the distance between pixels $p(x_1, y_1, z_1)$ and $q(x_2, y_2, z_2)$. The Euclidean distance is defined as

$$d(p,q) = \sqrt{(x_1 - x_2)^2 + (y_1 - y_2)^2 + (z_1 - z_2)^2} \quad (1)$$

and the chessboard distance is defined as

$$d(p,q) = \max\left(|x_1 - x_2|, |y_1 - y_2|, |z_1 - z_2|\right) \quad (2).$$

For a pixel $p(x_1, y_1, z_1)$, its *26-connected neighbors* were defined as pixels with chessboard distance 1.

III. Methods

Fig. 1 shows the flowchart of the proposed algorithm for automatically detecting pleural objects. The proposed algorithm consists mainly of three basic units. First, the user browsed the CT image series along the axial view and defined a volume of interest (VOI). Based on all CT attenuations in the VOI, an optimal threshold was derived using Otsu's method [10] to classify the pixels into foreground and background binarized groups. The foreground pixels were grouped into objects according to *26-connected neighbors*. Second, one of the formed objects was defined as the main object. Third, a pleura detection algorithm was recursively applied to verify the main object. The detected pleural object was deleted and

Shuo-Chueh Chen is with Division of Pulmonary and Critical Care Medicine, Department of Internal Medicine, China Medical University Hospital (CMUH), and with Graduate Institute of Clinical Medical Science, China Medical University (CMU), Taichung, Taiwan (e-mail: scchen18@gmail.com).

Su-Tso Yang is with Department of Radiology, CMUH and School of Chinese Medicine, CMU (e-mail: yangst@mail.cmu.edu.tw).

Yang-Hao Yu is with Division of Pulmonary and Critical Care Medicine, Department of Internal Medicine, CMUH and with Graduate Institute of Clinical Medical Science, School of Medicine, CMU (e-mail: yuchest71@gmail.com).

Chih-Yi Chen is with Cancer Center, CMUH (e-mail: micc@mail.cmuh.org.tw).

Wei-Chih Shen is with Department of Computer Science and Information Engineering, Asia University, Taichung, Taiwan. (phone: 886-4-22052121; fax: 886-4-22053425; e-mail: wcshen@gmail.com).

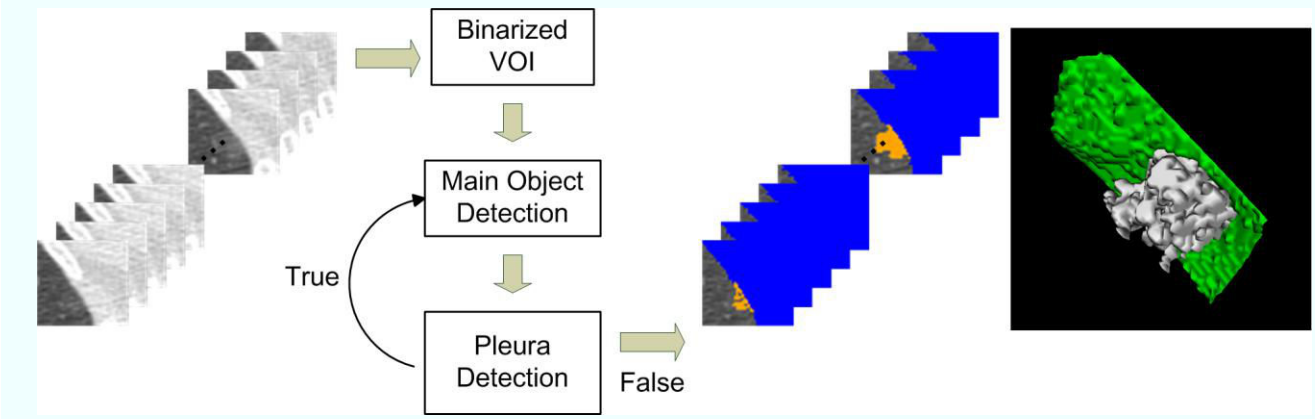

Figure 1. Overview of the pleura detection algorithm.

excluded from the objects in VOI, and a new main object was selected. The algorithm was stopped if the main object did not contain the pleura. The details of main object detection and pleura detection are described below.

A. *Main object detection*

An object with the largest radius of all the formed objects from the initial partition was defined as the main object. A 3D distance map with the same VOI size was constructed to describe the morphology characteristics of all the objects. For each pixel in the VOI, the chessboard distance to the nearest background pixel was calculated as its distance value for constructing the 3D distance map. For each object, the contained pixel with the largest distance value was defined as the center of the object and the distance is defined as the radius.

B. *Pleura detection*

The algorithm for pleura detection was derived based on a curve-fitting method and the measurement of the quality of the fitting curve. The curve was defined by a quadratic function

$$y = ax^2 + bx + c \quad (3).$$

and used to distinguish the location of the pleura between the lung tissue and its surrounding objects. A nodule was separated from the contacting surface of the pleura if they were connected. To reduce the computational complexity, the binarized VOI was decomposed into continuous 2D planes along the axial direction. In each plane, the pixels located in the surface of the main object were grouped into a set S. According to the coordinates of pixels in S, the coefficients of the curve function, a, b, and c, were calculated using the least squares method. The average Euclidean distance from all pixels of S to the fitting curve was calculated to measure the curve fit quality.

The pleura detection algorithm is described in pseudo code as follows:

Step 1) Find the sets S for the inputted plane and S' for the rotated inputted plane.

Step 2) Fit two curves using the S and S' sets and measure the fitting qualities. If the fit quality of the S' curve is superior to the other curve, replace the set S and its inputted plane by the set S' and its rotated inputted plane.

Step 3) While (the average Euclidean distance in the quality measurement $>$ 1)

{

Step 4) The pixels in the inputted plane are partitioned into two groups G1 and G2 by the curve. For each group, the probability for predicting as a foreground area is measured as

$$P(G_i) = \frac{\text{Number of pixels in the intersection of main object and } G_i}{\text{Number of pixels in } G_i},$$

where i=1 or 2 (4).

The group with the higher probability is predicted as the foreground area, and the other is a background area.

Step 5) The pixels in set S and in the main object are deleted if they are located in the predicted background area.

Step 6) According to the modified S, a new fitting curve is derived.

}

Fig. 2 shows the pleura detection processes conducted on three nodules. Because the axis of symmetry on the parabola of the fitting curve is parallel to the y-axis, two curves were fitted onto the inputted plane and the rotated plane, as described in Step 2. The curve with the best quality was adopted in the later analysis. For pleura detection, the final predicted foreground area acquired in Step 4 was used to verify the presence of the pleural object. The main object did not contain a pleura if it was almost entirely deleted, indicating the $P(G_i)$ was relatively low (R1 of Fig. 2). In contrast, a pleural object would be preserved in the predicted foreground area (R2 of Fig. 2). The pixels subtracting the original main object from the pleural object were regrouped and defined as new objects, and the detected pleural object was excluded from the VOI. Thereafter, the process repeated the previous method for selecting a new main object. When the inputted plane only contained a pleural object, the main object would be empty. The proposed pleura detection was flexible even if the nodule contacted several objects (R3 of Fig. 2). A nodule that contacted the chest wall and diaphragm was selected as the main object, and the chest wall was detected and

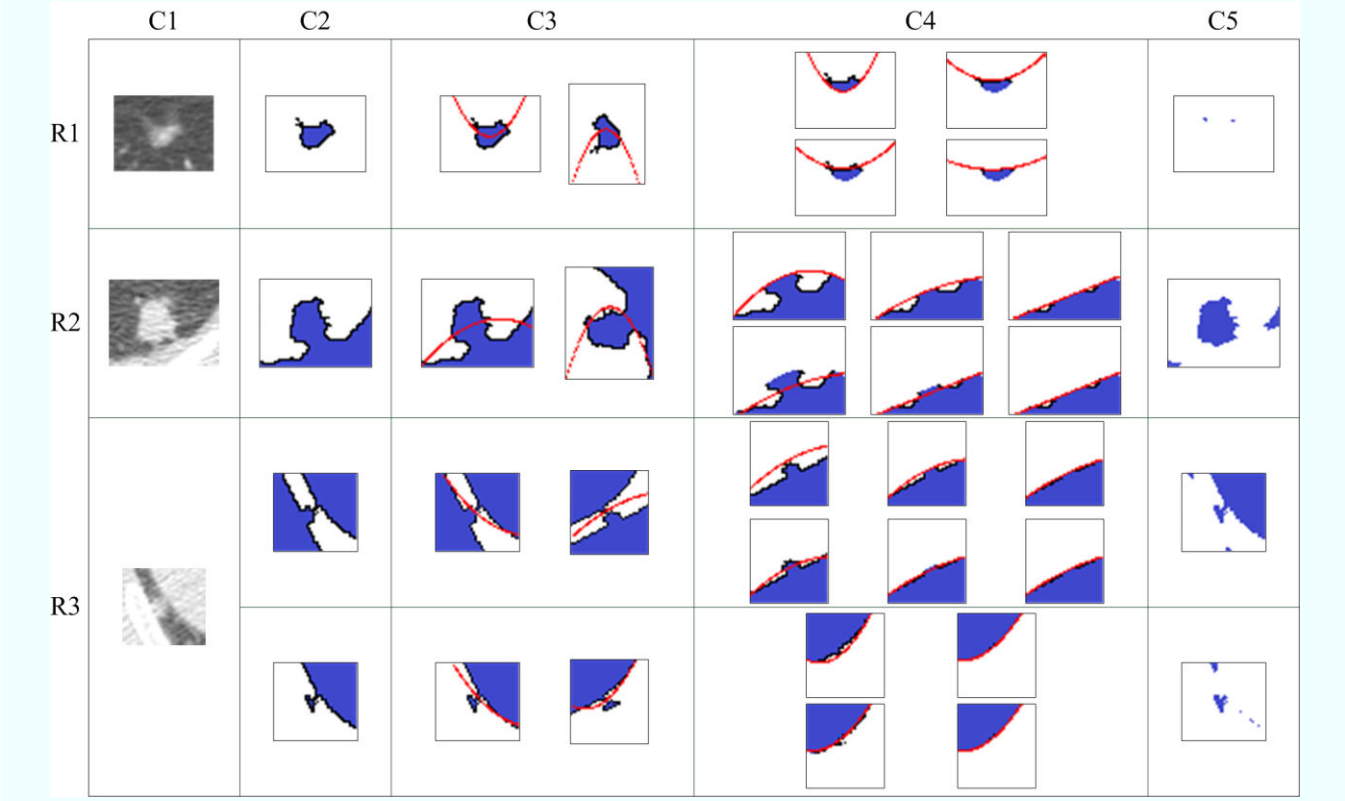

Figure 2. Examples for detecting pleura in an inputted ROI. R1: A nodule is surrounded by lung tissue. R2: A pleura-tagged nodule. R3: A nodule was located between the chest wall and diaphragm. The chest wall and diaphragm were detected and excluded in the first (upper row) and second round (lower row), respectively. C1: Inputted 2D ROI. C2: The main object. Blue = main object, black = set S. C3: Two possible fitting curves (red) were fitted for the set *S* of the inputted plane and the set *S'* of the rotated plane. C4: An iteration of the process for deleting the pixels of the main object and set S located in the predicted background (upper row), and fitting a new curve by the modified set *S* (lower row), is shown in a column. Multiple iterations were performed repeatedly until the stop criteria were met. C5: The remaining object was used to verify the existence of pleural objects in ROI.

eliminated in the first round. The nodule that was in contact with the diaphragm was selected as the main object, and the diaphragm was detected and eliminated in the second round. Thereafter, the nodule was separated from the chest wall and the diaphragm and selected as the main object in the last round.

IV. Experimental Results

It was difficult to obtain a consistent gold standard for defining the borders of pleural objects in CT images because of the inter-observer and intra-observer differences between the manually outlined objects. The segmentation results of the proposed algorithm were visually inspected by the attending physicians for any segmentation errors. The inspection mainly concerned the separation between nodule and pleural objects rather than the integrity of the pleural surface.

The database contained 64 CT image series of patients who underwent a health examination. The X-ray tube current used in the examination ranged from 20 to 50 mA. The slice thickness in each series was either 0.625 mm or 1.25 mm. A total of 96 nodules were detected in 64 patients. Of the 96 original nodules, 40 nodules in 864 images were included in the experiment because they were adjacent to (less than 3 cm) or contacted the surface of the chest wall or diaphragm. In total, 93.6% of the segmentation results were accepted in the inspection.

Fig. 3 shows two examples for separating the nodule from the contacted surface of pleural objects. The first nodule contacted the surface of chest wall (Fig. 3(a)). The second nodule contacted the surfaces of the chest wall and diaphragm (Fig. 3(b)). The proposed algorithm successfully separated the nodule from the pleural objects in each 2D plane, irrespective of contiguousness or isolation. In both nodules, volume rendering was provided to show the complexity of the nodule that contacted the pleural objects.

V. Discussion

The proposed algorithm detected the parietal and visceral pleurae surface that slid smoothly against each other during respiration. Even if the nodule came in contact with the surface of the pleural objects, they were separated by the fitting curve. The contacted area between the nodule and pleural objects enabled the objective assessment of the pleural invasion for evaluating the patient outcomes. In the current widely-used methods for evaluating pleural invasion, the assessment criteria are developed using a thick 2D CT image, and the evaluation depends highly on physician experiences.

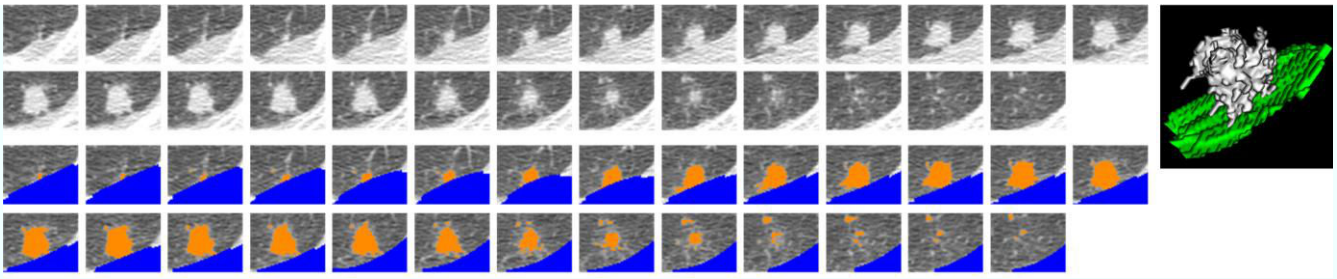

(a)

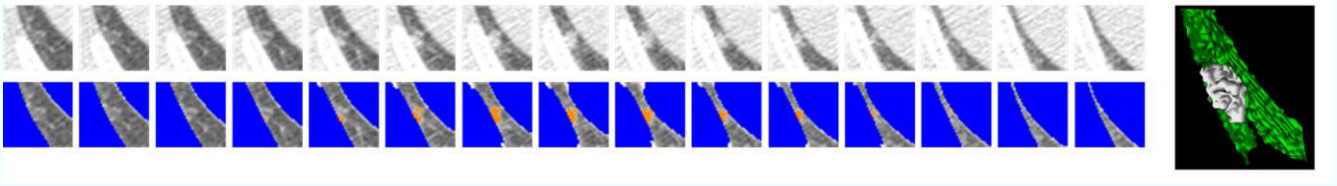

(b)

Figure 3. The results of pleura detection in continuous ROIs are shown in 2D and 3D views. (a) A pleura-tagged nodule. (b) A nodule was located between the chest wall and diaphragm.

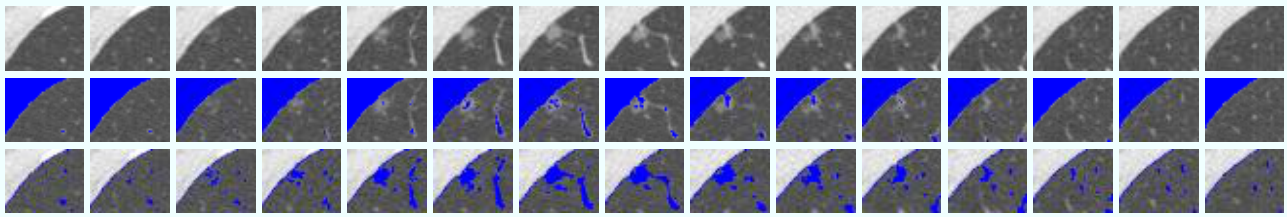

Figure 4. The exclusion of pleural objects improved the detection of the GGO nodule. The original image slices are shown in the first row. The detected main object (blue) is shown in the second row. The GGO component of the nodule was classified in the background. When the pleural object was excluded from VOI, a new threshold was derived using the CT attenuations of the remaining main object and background pixels. The new threshold detected the entire GGO nodule from the background.

The exclusion of pleural objects enabled the detection of the GGO nodule based on the CT attenuations shown in Fig. 4. In user-defined VOI, the CT attenuations of pleural objects were obviously higher than those of lung tissue, vascular networks, bronchioles, and nodules. When a threshold was derived using all CT attenuations of VOI, the threshold was mainly determined by the pleural objects and lung tissue, and may be overestimated for GGO nodule detection. Thus, the pleural objects could be excluded from VOI to derive a new optimal threshold using the remaining foreground objects and lung tissue. The new threshold could be used to detect the slight differences between the GGO nodule and lung tissue.

ACKNOWLEDGMENT

This work was supported by the Taiwan Department of Health, China Medical University Hospital Cancer Research Center of Excellence (DOH102-TD-C-111-005) and the National Science Council, Executive Yuan, Taiwan (NSC 101-2221-E-468-005-MY2).

REFERENCES

[1] National Lung Screening Trial Research Team, Aberle DR, Adams AM, Berg CD, Black WC, Clapp JD, Fagerstrom RM, Gareen IF, Gatsonis C, Marcus PM, Sicks JD. Reduced lung-cancer mortality with low-dose computed tomographic screening. N Engl J Med. 2011 Aug 4;365(5):395-409.

[2] Henschke CI, Yankelevitz DF, Mirtcheva R, McGuinness G, McCauley D, Miettinen OS; ELCAP Group. CT screening for lung cancer: frequency and significance of part-solid and nonsolid nodules. AJR Am J Roentgenol. 2002 May;178(5):1053-7.

[3] Austin JH, Müller NL, Friedman PJ, Hansell DM, Naidich DP, Remy-Jardin M, Webb WR, Zerhouni EA. Glossary of terms for CT of the lungs: recommendations of the Nomenclature Committee of the Fleischner Society. Radiology. 1996 Aug;200(2):327-31.

[4] Kakinuma R, Ashizawa K, Kuriyama K, Fukushima A, Ishikawa H, Kamiya H, Koizumi N, Maruyama Y, Minami K, Nitta N, Oda S, Oshiro Y, Kusumoto M, Murayama S, Murata K, Muramatsu Y, Moriyama N. Measurement of focal ground-glass opacity diameters on CT images: interobserver agreement in regard to identifying increases in the size of ground-glass opacities. Acad Radiol. 2012 Apr;19(4):389-94.

[5] Pennes DR, Glazer GM, Wimbish KJ, Gross BH, Long RW, Orringer MB. Chest wall invasion by lung cancer: limitations of CT evaluation. AJR Am J Roentgenol. 1985 Mar;144(3):507-11.

[6] A. Farag, A. El-Baz, G. G. Gimelfarb, R. Falk, and S. G. Hushek. Automatic detection and recognition of lung abnormalities in helical CT images using deformable templates. Lecture Notes in Computer Science, Medical Image Computing and Computer-Assisted Intervention, vol. 3217, New York: Springer-Verlag, 2004, pp.856–864.

[7] Lee Y, Hara T, Fujita H, Itoh S, Ishigaki T. Automated detection of pulmonary nodules in helical CT images based on an improved template-matching technique. IEEE Trans Med Imaging. 2001 Jul;20(7):595-604.

[8] Dehmeshki J, Amin H, Valdivieso M, Ye X. Segmentation of pulmonary nodules in thoracic CT scans: a region growing approach. IEEE Trans Med Imaging. 2008 Apr;27(4):467-80.

[9] Paik DS, Beaulieu CF, Rubin GD, Acar B, Jeffrey RB Jr, Yee J, Dey J, Napel S. Surface normal overlap: a computer-aided detection algorithm with application to colonic polyps and lung nodules in helical CT. IEEE Trans Med Imaging. 2004 Jun;23(6):661-75.

[10] Otsu, N. A threshold selection method from gray-level histograms. IEEE Trans. Systems, Man, and Cybernetics, 9(1), pp. 62-66.